RESEARCH ARTICLE

1-Azathioxanthone Appended Lanthanide(III) DO3A Complexes that Luminesce following Excitation at 405 nm.

Lea Gundorff Nielsen,[a,b] Anne Katrine Ravnsborg Hansen,[a] Patrycja Stachelek,[b] Robert Pal[b] & Thomas Just Sørensen*[a]

[a] Dr. L. G. Nielsen, Dr. A. K. R. Hansen, Prof. Dr. T. J. SørensenDepartment
Department of Chemistry & Nano-Science Center, University of Copenhagen Institution
Universitetsparken 5, DK2100 København Ø, Denmark
tjs@chem.ku.dk

[b] Dr. P. Stachelek, Prof. Dr. R. Pal, Department
Department of Chemistry, Durham University
South Road, Durham, United Kingdom, DH1 3LE
robert.pal@durham.ac.uk

Supporting information for this article is given via a link at the end of the document

Abstract: Since the pioneering report by Selvin, we have been fascinated by the potential of using lanthanide luminescence in bioimaging. The uniquely narrow emission lines and long luminescence lifetimes both provide the potential for background free images together with full certainty of probe localization. General use of lanthanide based bioimaging was first challenged by low brightness, and later by the need of UV (<405 nm) excitation sources not present in commercial microscopes. Here, we designed three lanthanide-based imaging probes based on a known motif to investigate the limitations of 405 nm excitation. These were synthesized, characterized, investigated on dedicated as well as commercial microscopes, and the photophysics was explored in detail. It was proven without doubt that the lanthanide complexes enter the cells and luminesce internally. Even so, no lanthanide luminescence were recovered on the commercial microscopes. Thus, we returned to the photophysical properties that afforded the conclusion that—despite the advances in light sources and photodetectors—we need new designs that can give us brighter lanthanide complexes before bioimaging with lanthanide luminescence becomes something that is readily done.

Introduction

Optical bioimaging is a central tool in life science.[1] Fluorescence microscopy provides information on both structure and function, but relies on fluorescent probes, either of biological origin or introduced as small molecules.[2] In commercial microscopes, the quality of the images is directly proportional to the brightness of the probe. Thus, high brightness organic and biological fluorescent probes dominate optical bioimaging.[3] Two paths exist for increasing the image quality: improving dyes or improving the detection efficiency of the microscope. In the research laboratories laser excitation sources and optical detectors, where each pixel has single photon sensitivity, are common. Indeed, most commercial microscopes have these capabilities. Thus, probe development should provide the biggest potential for improvement. While the organic fluorescent probes that are commonly used have been optimized by first Drexhage,[4] Haugland,[5] and more recently Lavis,[6] other emitters—disregarding fluorescent proteins—are still to find widespread use in optical bioimaging.[3b] Since the early work by Weissman, Elster, Beverloo, Selvin, Beeby, and Faulkner,[7] the narrow emission band, long luminescence lifetime, and emission in the near-IR have made lanthanide luminescence interesting for bioimaging applications.[7a, 8] Indeed, named classes of lanthanide based probes have been reported.[9] Even so, challenges remain for the exploitation of lanthanide based luminescent probes.[10] The lanthanide centered optical transitions are all forbidden, which is the origin of the long luminescence lifetimes, but also dictate very low molar absorption coefficients ($\varepsilon \leq 1$ cm^{-1} M^{-1}) *i.e.* a low brightness. This can be circumvented by sensitization by organic chromophores,[7d, 11] where the excited state of the antenna chromophore is higher in energy than the emitting state of the lanthanide(III) ion. Using primarily europium(III) luminescence and dedicated microscopes,[12] the benefits of the narrow emission lines and the long luminescence lifetime have been amply demonstrated.[13] Often 355 nm (3rd Harmonic of Nd:YAG) excitation is used, which requires microscopes with quartz optics. Further, excitation using continuous wave excitation with a 355 nm laser can be highly phototoxic. Two-photon excitation was developed to avoid the issues with high UV-exposure,[13a, 14] and while similar demonstrations of the benefits of using lanthanide based probes were reported, this method also require customized microscopes. Note, that the phototoxicity depends on both wavelength and radiation dose. Thus, excitation at NIR wavelength but with high intensity can be considered more harmful to cells compared to pulsed UV lasers with low repetition rates.[15] Following the availability of wavelength resolved detectors in commercial microscopes, we used a research microscope to show how spectral imaging can give rise to background free images.[16] We moved on to show that bioimaging following direct excitation of $\varepsilon \leq 0.1$ cm^{-1} M^{-1} bands was feasible on this dedicated platform.[17] As commercial microscopes now come equipped with highly sensitive detectors and powerful lasers light sources, we set out to demonstrate that now is the time for lanthanide based probes to shine throughout the life sciences.

When creating a lanthanide based luminescent probe, two pre-requisites have to be met: 1) the probe must sensitized following excitation of an antenna chromophore using the blue 405 nm laser

line. And 2) the probe must be stable in biological media. The latter is readily ensured by using kinetically inert lanthanide binding pockets,[18] while selecting a suitable chromophore is aided by the significant contribution of Parker and co-workers.[13b] Thus, we chose to make the Eu(III) complexes of the 1-azathioxanthone appended 1,4,7,10-tetraazacyclododecane 1,4,7-triacetic acid (DO3A) ligands shown in Figure 1. These complexes are based on the very well known design of adding a fourth arm to the DO3A scaffold, while the chromosphere was selected in the literature as the one that has been reported as the most promising candidate for lanthanide based bioimaging.

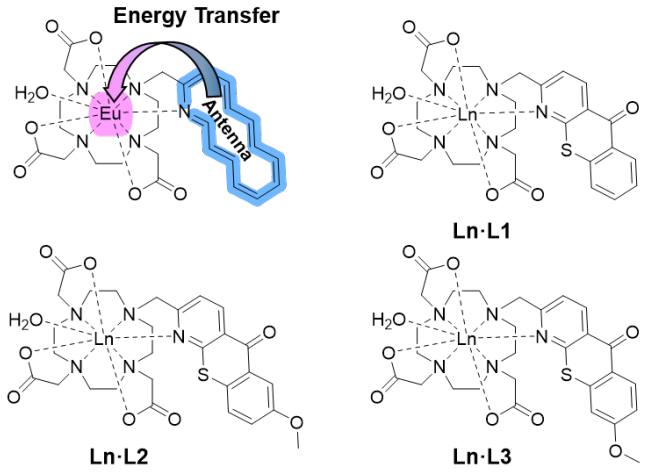

Figure 1: Illustration of the energy transfer to the Eu(III) center from the antenna and the chemical structure of the investigated Ln(III) complexes with the ligands **L1, L2** and **L3. The blue 'antenna' could be interpreted as an anthracene**

The choice of the thioxanthone chromophore class was further aided by the fact that we can use Dewar's rules to predict the effect of substituents and thus tailor the desired photophysical properties.[19] As the photophysics are known to change, when the chromophore is incorporated in a lanthanide(III) ligand and we know that they will change when we go to water, we synthesized three ligands: **L1**, **L2**, and **L3**. To fully understand these ligand systems, complexes were made with europium(III) targeting bioimaging, and with yttrium(III), terbium(III) and gadolinium(III) to determine the intricate photophysics of the excited energy transfer cascade that leads to the europium(III) luminescence.[25] The solution structure and photophysical properties of these twelve complexes were investigated in methanol and aqueous buffered. The effect of biological proteins were tested and live cell and fixed cell imaging were done on commercial and dedicated microscopes.

We found that the Ln(III) complexes with the ligands **L1**, **L2** and **L3** have similar if not identical solution structure, and that the intrinsic photophysical properties were unique to each ligand in a specific solvent system. And we found that the brightness of these lanthanide based probes at the point of excitation are low compared to fluorescence probes, but better than any other lanthanide probe when using 405 nm excitation. The tested europium(III) complexes were shown to stain cells, both live, dead and permeabilized, and beautiful cell images were recorded on microscopes dedicated to detecting lanthanide emission. However, when the same protocols were used at a facility for conventional optical bioimaging, no lanthanide emission was recovered. Following several control and model studies, it was concluded that commercial microscopes currently are biased against using lanthanide luminescence based probes. And as photophysical properties are governed by intrinsic details in structure, intramolecular distances, solvent effects and more, we must conclude that we do not have a clear path to efficient lanthanide based bioimaging probes that work well across all biological media.

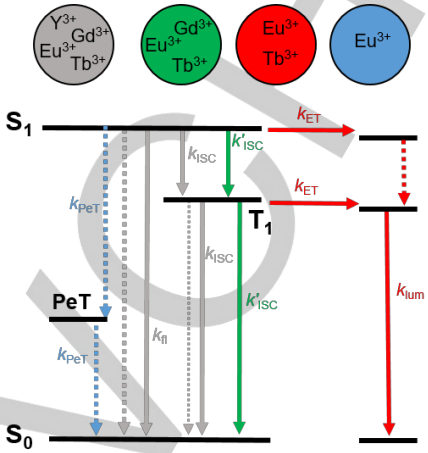

Figure 2: Simplified Jablonski scheme illustrating the different deactivation pathways possible upon excitation to S_1 of the antenna. Processes available for all the Ln(III) complexes with the ligands **L1, L2** and **L3** are shown in grey, additional processes induced by the lanthanide ions are marked with green (k'_{ISC}), energy transfer possible only to Eu(III) and Tb(III) is marked with red (k_{EnT}), and finally PeT quenching to Eu(II) is shown with blue (k_{PeT}).

Results and Discussion

Synthesis and characterization

The three 1-azathioxantone derivatives were synthesized following literature procedure through a two-step reaction.[19c] Bromination in the α-position on 2-methyl-1-azathioxanone has previously been described in the literature using a Wohl—Ziegler bromination.[20] However, it was not possible to reproduce this reaction in our labs. Though multiple modifications were attempted in the reaction conditions, the reaction either did not yield the desired molecules in high enough yields to continue the synthetic procedures or gave undesired products. As an alternative, a patent describing functionalization of the α-position was used with minor modifications, see ESI for experimental details.[20b, 21] In the preferred procedure, see Scheme 1, the parent 2-methyl-1-azathioxanthone derivatives were oxidized using iodide, iron(III)sulphate, TFA, and *tert*-butyl iodide in DMSO. The reaction was performed at least three times for each derivative, and it was shown that *tert*-butyl iodide is not required for the oxidation to occur. The reaction yields a mixture of the desired alcohol (7-9) as the minor product and the aldehyde (7a-9a) as the major product. The reaction mixture, containing both alcohol and aldehyde, was taken directly to the next step, where lithium borohydride with trimethylsilyl chloride in THF were used to reduce the sulfone and the aldehyde of the major product (7a-9a). Following the reduction, the alcohol (7-9) was isolated after aqueous workup in an overall yield between 40-50 %. To introduce a better leaving group, the alcohol was treated with methanesulfonyl chloride, and the reactive chromophores (10-12) were isolated in acceptable yields by chromatography. The chromophore was attached to the kinetically inert DO3A-scaffold

using K_2CO_3 in acetonitrile. After removal of the *tert*-butyl esters using trifluoroacetic acid, the ligands **L1**, **L2** and **L3** were isolated by tituration. Finally, the Ln(III) complexes **Ln·L1**, **Ln·L2**, and **Ln·L3** were formed by complexation in a 1:1 mixture of H_2O and MeCN at neutral pH using the appropriate lanthanide(III)chloride as the Ln(III) source. For complexation Y(III), Gd(III), Tb(III) and Eu(III) were used. The complexes were isolated following de-salting on a sephadex PD-10 column. The complexation is assumed to be quantitative, but no yields are reported as the highly hygroscopic compounds does not allow for accurate determination of absolute purity or recovered mass.[22] The formation of the Eu(III) complexes were confirmed with ^{1}H-NMR, mass spectrometry, and luminescence spectroscopy (see ESI for details).

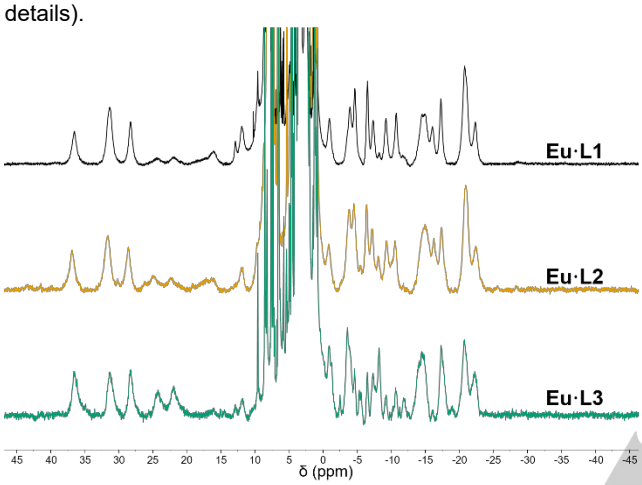

Figure 3: Paramagnetic ^{1}H-NMR of **Eu·L1** (top), **Eu·L2** (middle) and **Eu·L3** (bottom) in DMSO-d_6 at 27 °C.

Solution Structure

Figure 3 shows the paramagnetic ^{1}H-NMR spectra of the **Eu·L1**, **Eu·L2**, and **Eu·L3** complexes recorded in DMSO-d_6. Paramagnetic ^{1}H-NMR spectra of lanthanide complexes with DOTA and DO3A-like ligands are well understood and have been characterized in detail previously.[23] The spectra in Figure 3 show similar characteristics and are consistent with reported spectra of eight-coordinated unsymmetrical Eu(III) complexes with three coordinating carboxylate arms on a cyclen backbone.[24] Due to the constrained conformation of an eight-coordinated complex, fast exchange between different forms are restricted resulting in resolution of the axial protons in the cyclen ring (25 -35 ppm).[23a] The NMR spectra clearly show that the Eu(III) binding pocket is similar in all three complexes.

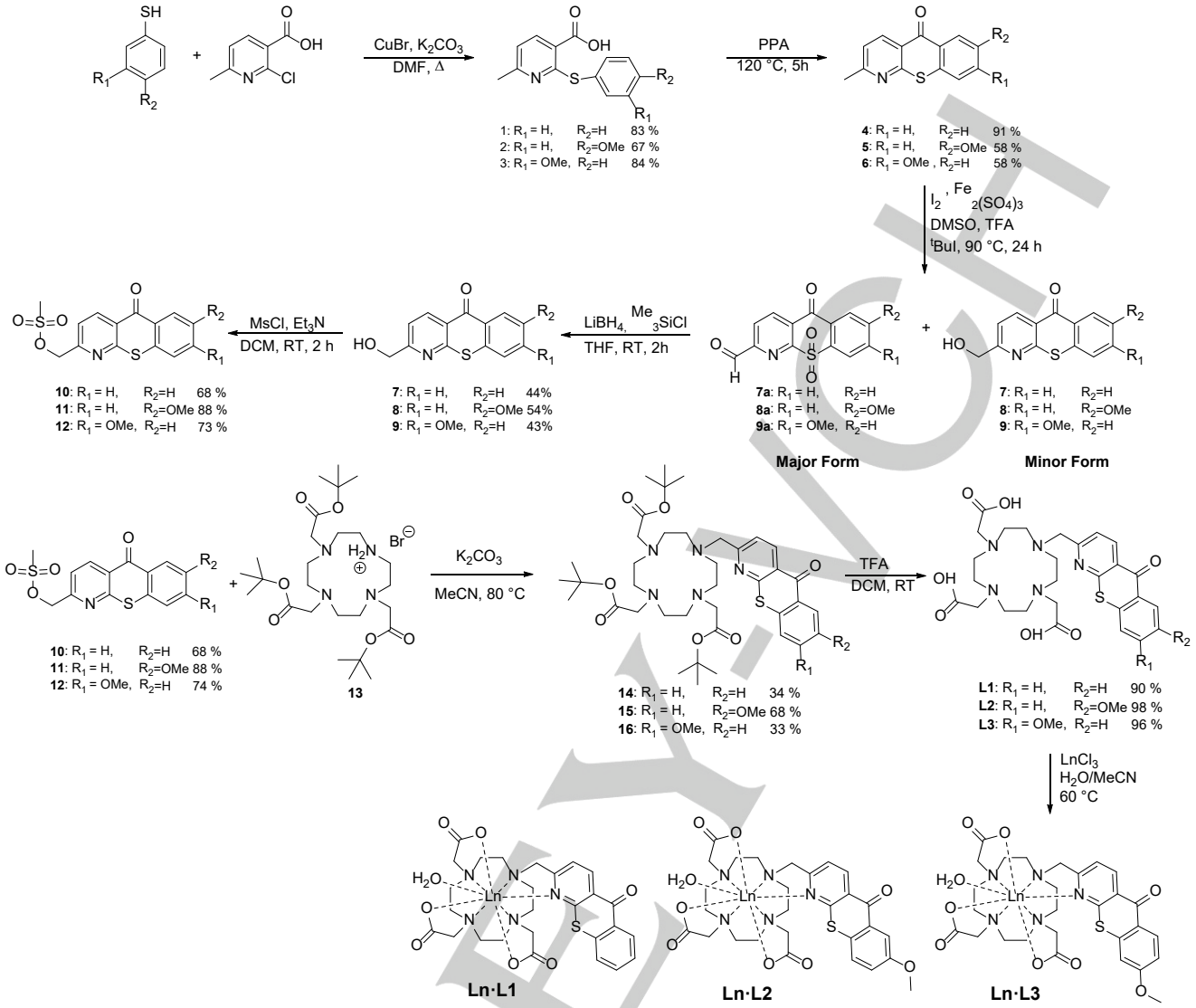

Scheme 1. Synthetic pathway to Ln(III) complex **Ln·L1**, **Ln·L2**, and **Ln·L3**.

Table 1: Luminescence lifetimes determined for **Eu·L1** in MeOH and MeOD and calculated number of solvent molecules. Excited at 380 nm, emission collected at 702 nm.

	Eu·L1
τ_{obs}^{Ln} MeOH (ms)	0.804
τ_{obs}^{Ln} MeOD (ms)	1.645
q (number of "H_2O")	0.463
***q* (number of MeOH)**	0.93 ~ 1

For the complexes based on **L1**, **L2**, and **L3** both an open and closed configuration is possible in solution where the difference is the coordination from the pyridine unit directly to the Ln(III), as previously reported.[25] The paramagnetic NMR spectra of the Eu(III) complexes obtained in DMSO-d_6 indicate that the ligands are mainly octadentate. However, two short components were determined in the fluorescence lifetimes of the antenna chromophore in methanol, see below. This indicates the presence of two different conformations in solution on the timescale of the fluorescence lifetime (a few nanoseconds). The luminescence lifetimes of **Eu·L1** were determined in methanol and deuterated methanol (CH_3OD). The results are reported in Table 1. From the luminescence lifetimes an average number of solvent molecules can be determined using the modified Horrocks equation as described in the ESI.

For **Eu·L1** only one lifetime was determined from the time-resolved Eu(III) luminescence decay profile. The number of methanol molecules determined to coordinate to the central ion is *q* = 0.93, which is what would be expected for an octadentate ligand. Note that *q* carries an error of ± 0.5. If we consider the timescale of the fluorescence (ns) and luminescence (ms), it is much shorter for the fluorescence. Thus, the exchange rate for the equilibria between open and closed form is in between the timescale of the two experiments, and we see two species in the fluorescence lifetime and only one in the luminescence lifetimes.

Photophysical properties in MeOH

The absorption spectra of all the 12 complexes measured in methanol are shown in Figure 4. The spectra are spilt into three distinct absorbance spectra determined by the antenna on the complex. For the same ligand framework, only small difference in

the UV-region are seen between the different Ln(III) ions. No Ln(III) specific bands are observed. The absorbance spectra are very similar to the reported absorbance for the parent chromophores and the features specific to each chromophore derivative are also observed for the Ln(III) complexes.[19c]

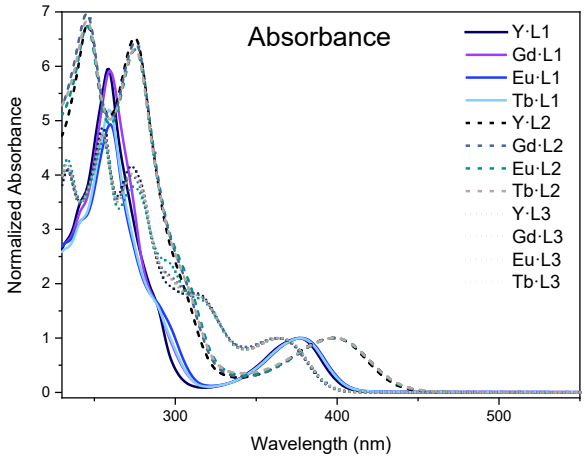

Figure 4: Normalized absorption spectra of the Ln(III) complexes with **L1**, **L2**, and **L3** in MeOH at $1.5 \cdot 10^{-5}$ M. The complexes are with Y(III) (black), Gd(III) (purple), Eu(III) (green) and Tb(III) (beige).

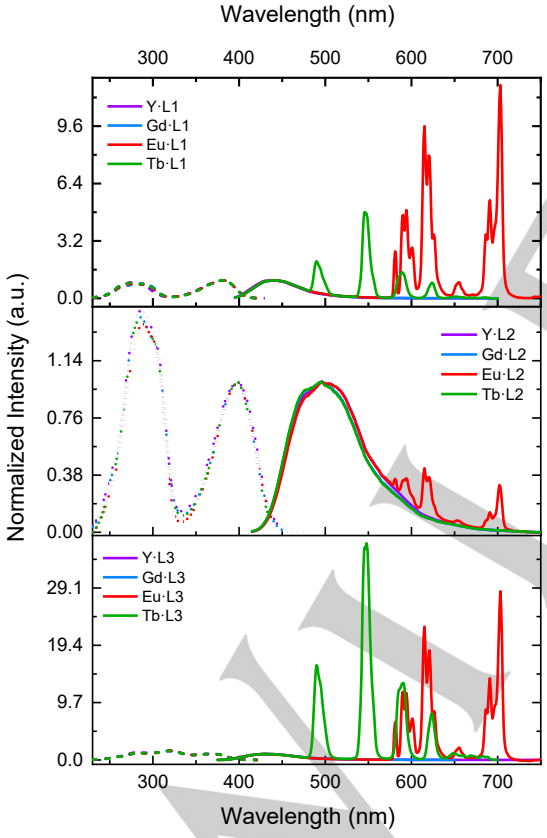

Figure 5: Normalized excitation (dashed) and emission (solid) spectra of Y (purple), Gd (blue), Eu (red), and Tb (green) in methanol, 1.5·10-5 M. complexated with L1 (top, λ_{em} 440 nm, λ_{ex} 380 nm), L2 (middle, λ_{em} 500 nm, λ_{ex} 397 nm), and L3 (bottom, λ_{em} 435 nm, λ_{ex} 365 nm)

The absorption spectra, all display strong absorption in the UV range with 2-3 bands in the range of 300—400 nm. The complexes with **L1** have two bands in the range from 300—400 nm, and the primary absorption band at a maximum of 377 nm. This is a 7 nm redshift compared to the 1-azathioxanthone. The absorption spectra of the complexes with ligand **L3** show that the primary absorption band has a maximum of 364 nm, which is a blueshift of 5 nm compared to the parent chromophore. The data reveals that the addition of the electron donating methoxide group in the para-position to the carbonyl group i.e. going from **L1** to **L3**, induces a blueshift of the primary ππ* transition and creates a close lying nπ* state at 315 nm. This was also seen in the parent chromophore.[19c, 26] In the complexes with **L2**, the methoxy substituent is in the para-position to the bridging sulfur atom. This induces a redshift of the absorption maximum and creates a chromophore with a maximum absorption at 399 nm.

The excitation and emission spectra measured for all the complexes are reported in Figure 5. The excitation spectra are identical for all four Ln(III) ions within one ligand scaffold and match the primary features of the absorption spectra of the respective complexes in Figure 4. The emission from the antenna-centered fluorescence, in the region of 400-600 nm, is independent of the central Ln(III) ions. Thus, it is clear that the coordination of a trivalent Ln(III) does not influence the energetics of the ligand-centered excited state. The same is true for the phosphorescence spectra measured for the Gd(III) complexes shown in the ESI. On the red side of the ligand fluorescence, the characteristic Ln(III) luminescence is observed from Eu(III) and Tb(III), which are the two used Ln(III) ions with relevant accepting energy levels.

Excited state energy overlap

A prerequisite for efficient lanthanide sensitization is energy overlap between donor and acceptor states. Generally, in the field of lanthanide luminescence, the energy match has been evaluated by comparing the determined energies of the excited states of the antenna and Ln(III) ion. Thus, the relative energies of the excited states involved in the energy transfer cascade leading to the lanthanide-centered luminescence are compared directly as shown in Figure 6. The excited energy levels of the chromophore are expected to be identical for all four complexes, as documented in Figure 4. A general design rule reported in the literature states that the optimal energy gap from the donating state to the emitting/receiving lanthanide state should be between 2000 cm^{-1} to 3500 cm^{-1}.[27]

The energy transfer from the antenna to the Ln(III) ion most likely occurs through a Dexter or FRET-type mechanism. The efficiency of both mechanisms depends on the spectral overlap between the emission of the donor and the absorption spectrum of the acceptor.[28] However, due to the broad spectral features of organic chromophores, the overlap with the accepting Ln(III) state is poorly described using the lines of the excited states as illustrated in Figure 6. Instead, the actual absorption and emission profiles should be used to adequately describe the energy overlap. In Figure 7 the spectral overlap of the absorption of Eu(III) and Tb(III) with the fluorescence of the antenna in **L1** is visualized. The absorption of the Ln(III) ions are determined from 0.1 M triflate Ln(III)-salts in water. Note, that both the emission and absorption are normalized to illustrate the overlap of the bands with the energy and not to calculate the actual spectral overlap integral. From Figure 7, it is clear that there is a spectral overlap from the chromophore **L1** to multiple levels in the Eu(III) ion. There is an overlap with both the $^5D_1$, $^5D_2$, $^5D_3$, and even partly $^5L_6$ from the singlet state. Though back energy transfer and

quenching from PeT will affect the overall quantum yield, energy transfer from the singlet state can occur to multiple electronic states in Eu(III). For Tb(III) only one electronic state has a spectral overlap with the fluorescence from the antenna. The higher luminescence quantum yield determined for Eu(III) (3%) compared to that of Tb(III) (1%) could be explained by the difference in spectral overlap to the two Ln(III) ions, see below. The spectral overlap from **L2** and **L3** are reported in the ESI. Because the excited state energy levels of **L3** are more blueshifted compared to **L1** and **L2** the spectral overlap is higher for both **Eu·L3** and **Tb·L3** and sensitization from both the singlet and triplet state is possible. For Tb(III) a small overlap with the $^5D_3$ state is possible. For both complexes with **L3**, the energy gap to the lowest emitting electronic state is also increased; reducing back energy transfer.

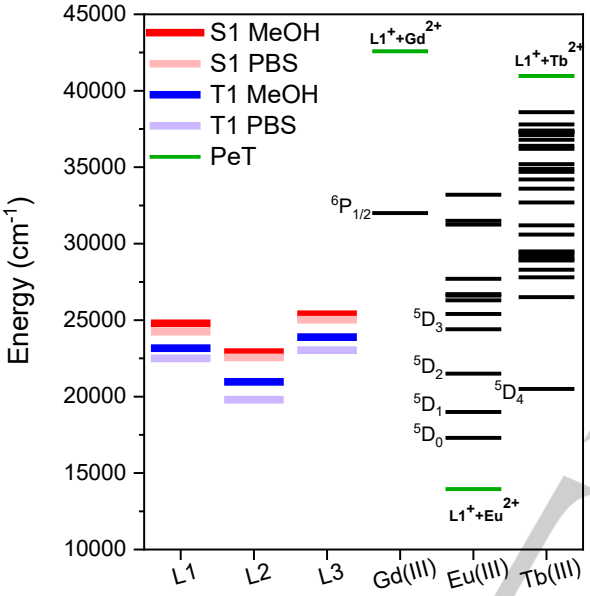

Figure 6: Energy diagram for **L1**, **L2**, and **L3** in MeOH and PBS together with the energy levels of Gd(III), Eu(III) and Tb(III).[29] Solid lines show excited singlet (red), triplet (blue), approximate redox level (green), and energy levels of Ln(III) ions (black). The reduction potentials used in the figure are EuIII/EuII = –0.35 V in water vs. NHE and for thioxanthone in DMF: 1.62 V vs. NHE.[20b, 30]

Excited State Processes

L1. The fluorescence and luminescence quantum yields of the complexes with **L1** were determined with coumarin153 as the reference dye using five samples at different concentrations as recommended by IUPAC.[31] The results for the samples are compiled in Table 2 together with photophysical properties of the emission and absorption spectra determined in methanol. The fluorescence quantum yields are decreased in the complexes compared to those of the free chromophores. Furthermore, a reduction is observed when the metal center is changed. From the Y(III) to the Gd(III) complexes a large reduction is observed. Here, the addition of a paramagnetic heavy element is dramatically increasing the non-radiative rates from S_1.

Energy transfer to Tb(III) from the S_1 state, can explain the difference between the quantum yield in Gd(III) complexes compared to Tb(III) complex. For **Tb·L2** no Tb(III) centered emission is observed due to the small energy gap from the lowest emitting level in Tb(III) to the S_1/T_1 state of the chromophore. For the Eu(III) complexes both energy transfer and PeT quenching is reducing the fluorescence quantum yield.

The fluorescence lifetimes were determined for the four different Ln(III) complexes in methanol and compared to the parent 1-axathioxanthone chromophore. Two short lifetimes were found in all of the complexes together with a long component with an almost insignificant amplitude (0.1-0.2%), see ESI. For the parent chromophore, only one lifetime was observed. Photophysical studies of collision between the 2-methyl-1-azathioxanthone antenna and different free Ln(III) ions have reported similar results.[26] Here, a short component arising from the S_1 state was found along with a long component assigned to room temperature phosphorescence. The long component was found to increase in amplitude as a function of increasing Ln(III) concentration. To investigate if the longer lifetime component originates from room temperature phosphorescence, a decay-associated spectrum (DAS) was obtained for **Gd·L5**, see ESI. In the normalized DAS spectrum, the emission spectrum of the long component can be compared against the two shorter components, where a redshift indicating the presence of room temperature phosphorescence is observed. The two other components have very similar emission profiles. Thus, the time-resolved data indicate that at least two different species are present in solution with τ_1 and τ_2 assigned as the fluorescence lifetime of possibly an open and closed complex structure.

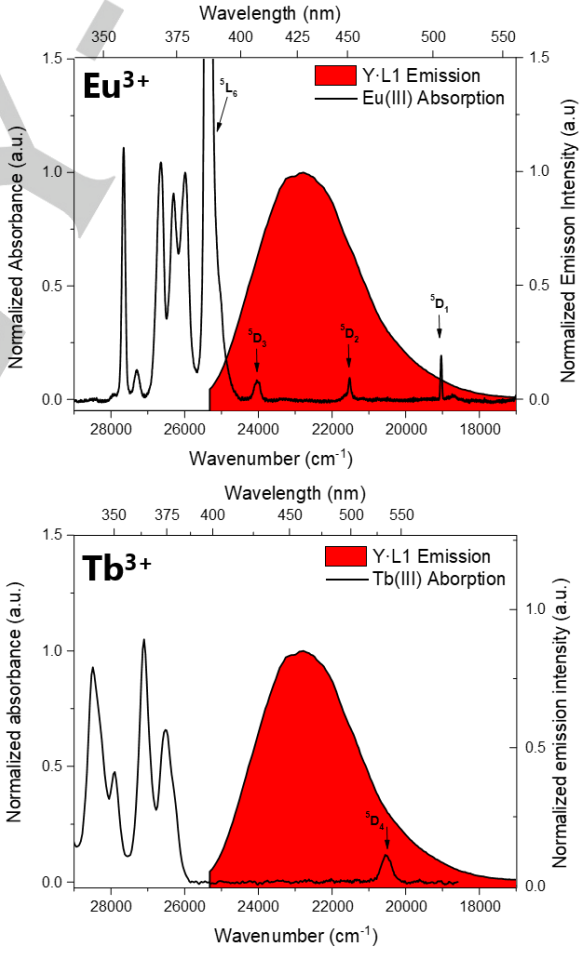

Figure 7: Spectral overlap between emission from **Y·L1** (red) with the absorption of 0.1 M $Eu(OTf)_3$ in water (top, black)[32] and 0.1 M $Tb(OTf)_3$ in water (bottom, black).[33] The relevant electronic states of the Ln(III) ions are reported.

To probe the excited state mechanisms, the rates of the excited state depopulation pathways were determined from the intensity

weighted fluorescence average lifetime and the florescence quantum yield, see Table 2.

Table 2: Photophysical properties and excited state rates of Ln(III) complexes with **L1** determined in MeOH.

	L1[19c]	**Y·L1**	**Gd·L1**	**Eu·L1**	**Tb·L1**
λ_{abs} (nm)	371	377	377	377	377
λ_{fl} (nm)	427	439	442	443	441
E_S (cm^{-1})	25340	24788	24715	24730	24741
E_T (cm^{-1})	23800	23170	23170	23380	23170
Φ_{fl} (%)	2.7	2.6	2.3	1.6	1.3
Φ_{lum}(%)				3.0	1.1
$<\tau_{obs}^{fl}>$ (ns)	0.57	0.644	0.632	0.481	0.566
τ_{rad}^{fl} (ns)	21	25	27	30	44
k_{obs}^{fl} (s^{-1})	$17.5\cdot10^8$	$15.5\cdot10^8$	$15.8\cdot10^8$	$20.8\cdot10^8$	$17.7\cdot10^8$
k_{rad}^{fl} (s^{-1})	$0.47\cdot10^8$	$0.40\cdot10^8$	$0.36\cdot10^8$	$0.33\cdot10^8$	$0.23\cdot10^8$
k_{nr}^{fl} (s^{-1})	$17.1\cdot10^8$	$15.2\cdot10^8$	$15.5\cdot10^8$	$20.5\cdot10^8$	$17.4\cdot10^8$
k_{ISC}^{fl} (s^{-1})[a]			$0.3\cdot10^8$	$0.3\cdot10^8$	$0.3\cdot10^8$
k_{EnT}^{fl} (s^{-1})[b]				$5.0\cdot10^8$	$1.9\cdot10^8$
k_{PeT}^{fl} (s^{-1})[c]					

[a]: $k_{ISC}^{fl} = k_{nr}^{fl}(Gd) - k_{nr}^{fl}(Y)$. [b]: $k_{EnT}^{fl}(Tb) = k_{nr}^{fl}(Tb) - k_{nr}^{fl}(Gd)$. [c]: $k_{EnT}^{fl}(Eu) + k_{PeT}^{fl}(Eu) = k_{nr}^{fl}(Eu) - k_{nr}^{fl}(Gd)$.

The excited state kinetics determined from the average fluorescence lifetimes show that there is an increase in the non-radiative rates for the Gd(III), Eu(III) and Tb(III) complexes relative to that of **Y·L1**–this is in accordance with the determined quantum yields. For **Tb·L1** quenching of the singlet state is increased further due to energy transfer to the Tb(III) center. Finally, for **Eu·L1** accelerated ISC, EnT to Eu(III), and PeT quenching all quench the chromophore S_1. A more efficient energy transfer is expected for Eu(III) compared to Tb(III) cf. Figure 7.

L2. The fluorescence and luminescence quantum yields for the complexes with **L2** are reported in Table 3 together with general photophysical properties determined in methanol. The fluorescence quantum yields are following the expected reduction when the central ion is changed. From **Y·L2** to **Gd·L2** a large reduction is observed. Here, the addition of a paramagnetic heavy element is dramatically increasing the non-radiative rates. As above, energy transfer to Tb(III) from the S_1 state can explain the difference between the quantum yield in **Gd·L2** compared to **Tb·L2**. However, due to the small energy gap, no Tb(III) centered emission is observed. For **Eu·L2** both energy transfer and PeT quenching reduce the fluorescence quantum yield.

Table 3: Photophysical properties of complexes with L2 determined in MeOH.

	L2[19c]	**Y·L2**	**Gd·L2**	**Eu·L2**	**Tb·L2**
λ_{abs} (nm)	390	399	399	399	399
λ_{fl} (nm)	468	496	496	496	496
E_S (cm^{-1})	23980	22910	22960	22940	23000
E_T (cm^{-1})	21650	20970	20970		
Φ_{fl} (%)	32	25.3	14.2	8.8	14.1
Φ_{lum}(%)				0.51	

Three fluorescent lifetimes were found in all of the Ln(III) complexes with **L2**, see ESI. For the parent chromophore, only one lifetime was observed. In contrast to **L1**, the longest determined lifetime is in the same range as the lifetime determined for the free chromophore, and the three lifetime components are also more evenly populated. Thus, the third lifetime does not appear to be due to the emission from a T_1 state. This is supported by the DAS spectra of **Gd·L2** that shows that the three components have almost identical emission profiles, which is in contrast to what was observed for **Gd·L1**, see ESI. In the photophysical studies of collision quenching between the 7-methoxy-2-methyl-1-azathioxanthone antenna and different free Ln(III) ions, no room temperature phosphorescence was observed, which is in agreement with the reported data here. For the free chromophore, a T_2 state has been described with near degeneracy to the S_1 state, which can account for one of the three lifetimes with identical spectra.[19c, 26] As the T_2 was significant, no attempt was made to calculate the excited state rates from the average fluorescence lifetimes.

L3. Finally, the fluorescence and luminescence quantum yields for the Ln(III) complexes with **L3** are reported in Table 4. For the complexes with ligand **L3**, quinine sulfate was used as the reference dye. For the parent chromophore large non-radiative rates together with low fluorescence quantum yields are observed.[19c] For the Ln(III) complexes with **L3** similar low fluorescence quantum yields were determined. However, as seen in the emission spectra in Figure 5, the Tb(III) and Eu(III) complexes show characteristic luminescence patterns with strong intensity. This is also reflected in the luminescence quantum yields reported in Table 4. Especially for Tb(III), a large luminescence quantum yield was observed.

Table 4: Photophysical properties and excited state rates of complexes with L3 determined in MeOH.

	L3[19c]	**Y·L3**	**Gd·L3**	**Eu·L3**	**Tb·L3**
λ_{abs} (nm)	359	364	364	364	364
λ_{fl} (nm)	409	431	430	430	430
E_S (cm^{-1})	26670	25380	25420	25400	25380
E_T (cm^{-1})	24270	23890	23890		
Φ_{fl} (%)	0.8	0.94	0.97	0.48	1.1
Φ_{lum}(%)				2.2	6.1
$<\tau_{obs}^{fl}>$ (ns)	0.27	0.353	0.328	0.284	0.296
τ_{rad}^{fl} (ns)	34	38	34	59	27
k_{obs}^{fl} (s^{-1})	$37\cdot10^8$	$28\cdot10^8$	$31\cdot10^8$	$35\cdot10^8$	$34\cdot10^8$
k_{rad}^{fl} (s^{-1})	$0.30\cdot10^8$	$0.27\cdot10^8$	$0.30\cdot10^8$	$0.17\cdot10^8$	$0.37\cdot10^8$
k_{nr}^{fl} (s^{-1})	$36.7\cdot10^8$	$28.1\cdot10^8$	$30.2\cdot10^8$	$35.0\cdot10^8$	$33.4\cdot10^8$
k_{ISC}^{fl} (s^{-1})[a]			$2.1\cdot10^8$	$2.1\cdot10^8$	$2.1\cdot10^8$
k_{EnT}^{fl} (s^{-1})				$4.8\cdot10^8$	$3.2\cdot10^8$
k_{PeT}^{fl} (s^{-1})					

Similar to the observations made for the complexes with **L1**, three lifetimes were found for the complexes with **L3**, see ESI. Again, two short components with a similar rate as for the free chromophore and one component with a longer lifetime. The third lifetime is only present in a very small population (0.1-0.6%), and the DAS spectra of **Gd·L3** showed the redshift in the emission profile of the long component that confirm it as arising from room temperature phosphorescence.

The excited state rates were determined based on the average lifetime of the two short components, see Table 4. A higher luminescence quantum yield was observed for **Tb·L3** compared

to **Eu·L3**. However, the non-radiative deactivation of **Eu·L3** was found to be larger than for **Tb·L3**. This could indicate efficient quenching of the excited state through PeT quenching, reducing the overall Eu(III) centered quantum yield, despite a good spectral overlap between **L3** and Eu(III).

Across the three ligands, the trends observed for the parent chromophores are retained for the respective Ln(III) complexes. The highest luminescence quantum yield and brightness is seen for **L1** and **L3**. However, the results showed that no single simple parameter can be tuned to obtain efficient Ln(III) sensitization. The efficiency depends on many different parameters such as: the rate of intersystem crossing, the energy gap from singlet to triplet state, the energy gap to Ln(III) states to chromophore cantered states, the spectral overlap, the solvatochromy of the chromophore, and several others. Further, the complex solution structure and the interaction of the complex and the media will also complicate the excited state mechanism, and even in a simple solvent system as methanol without ions and pH a difficult speciation profile was obtained.

Table 5: Photophysical properties of **Eu·L1**, **Eu·L2** and **Eu·L3** determined in PBS solution at pH 7.4. See ESI for details.

	1	**2**	**3**
λ_{abs} (nm)	382	403	369
λ_{fl} (nm)	452	517	440
$<\tau_{fl}>$ (ns)	3.67	8.3	0.61
ϕ_{fl} (%)	9.3	6.9	2.1
Φ_{lum}(%)	2.8	0.8	2.5
Log(ε) at λ_{max}	3.8	3.7	3.8
B at λ_{max}	188	44	174
Log(ε) at λ_{405}	3.0	3.7	2.0
B at λ_{405}	26	42	2.5
τ (H_2O) (ms)	0.604	0.256	0.539
τ (D_2O) (ms)	1.753	0.424	2.017
q	1.0 ±0.5	-	1.3 ±0.5

Antenna chromophore photophysics in biological media

In biological media, the photophysical properties of the investigated Ln(III)-complexes are altered. Effects from changes in pH and buffer system was evaluated in previously.[34] Here, the photophysical properties of **Eu·L1**, **Eu·L2**, and **Eu·L3** were investigated in PBS buffer (pH 7.4) at $1.5 \cdot 10^{-5}$ M and contrasted to the properties of the parent 1-azathioxanthone.[19c] Figure 8 shows the absorption spectra, which display strong absorption in the UV range with 2-3 bands in the range of 300—400 nm. **Eu·L1**, with no substituents on the azathioxanthone chromophore, has two bands in the range from 300—400 nm, and the primary absorption band of **Eu·L1** has a maximum of 382 nm. This 12 nm redshift compared to the 1-azathioxanthone, we assign primarily to solvatochromism.[19c] Figure 8 shows that the primary absorption band of **Eu·L3** has a maximum of 369 nm. The data reveals that the addition of the electron donating methoxide group in the para-position to the carbonyl group i.e. going from **Eu·L1** to **Eu·L3**, induces a blueshift of the primary ππ* transition and creates a close lying nπ* state at 315 nm. This was also seen in the parent chromophore.[19c, 35]

In **Eu·L2** the methoxy substituent is in the *para*-position to the bridging sulphur atom. This induces a redshift of the absorption maximum and creates a chromophore with a maximum absorption at 403 nm, close to the 405 nm central wavelength of the blue laser line commonly used in commercial microscopes.

Figure 8 shows that the excitation spectra of all three complexes exclusively show the primary band of the chromophore. No bands arising from direct excitation of the Eu(III) center can be seen. Further, the excitation spectra are identical to the absorption spectra. Note that the absorption spectrum of **Eu·L1** extends into the blue and can be excited using a 405 nm laser. All photophysical details of the antenna chromophores are compiled in Table 5 and the corresponding data can be found in the ESI. Note that the mirror image rule works for **Eu·L1** and **Eu·L3**, while a second band on the red side is seen for **Eu·L2**. This is assigned to ligand-centered phosphorescence.[19c, 35]

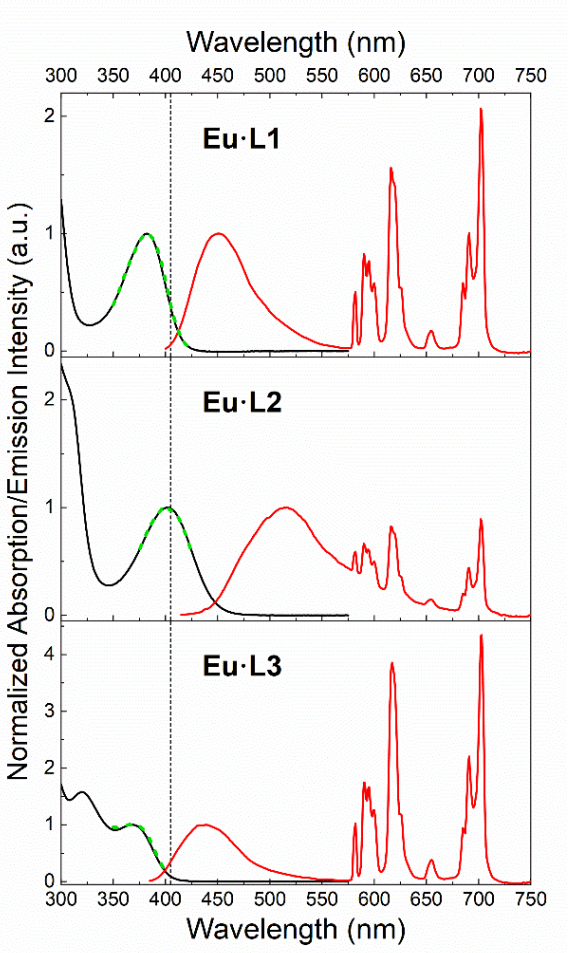

Figure 8: Normalized absorption (black), excitation (dashed green on top of absorption) and emission (red) spectra of **Eu·L1** (λ_{ex} 380 nm, λ_{em} 701 nm), **Eu·L2** (λ_{ex} 405 nm, λ_{em} 701 nm) and **Eu·L3** (λ_{ex} 370 nm, λ_{em} 701 nm) in PBS buffer pH 7.4 at $1.5 \cdot 10^{-5}$ M. The black vertical dashed line is positioned at 405 nm, to show the central excitation wavelength in a blue laser.

Eu(III) photophysics

The emission spectra shown in Figure 8 have the characteristic europium centered luminescence on the red side of the ligand fluorescence and phosphorescence. The narrow emission lines of the europium luminescence report on the local symmetry.[36] The fine structure is very similar in all three spectra, which confirms

the observation from NMR, that the three complexes have similar coordination geometry and solution structure.[23a, 24] A prerequisite for efficient lanthanide sensitization is energy overlap between donor and acceptor states. Thus, the relative energies of the excited states involved in the energy transfer cascade leading to the lanthanide-centered luminescence must be considered for the three complexes.

Back energy transfer from Eu(III) to the antenna chromophore is unlikely as the energy gap is higher than 2000 cm^{-1}. The luminescence lifetimes were measured in PBS (pH = 7.4) prepared from H_2O and D_2O to determine the number of solvent molecules coordinated to the Eu(III) center using the modified Horrocks equation.[37] The lifetimes of **Eu·L1** and **Eu·L3** are as expected, while the lifetime of **Eu·L2** is too short. This is assigned to back energy transfer to the triplet state T_1 2500 cm^{-1} over the $^5D_0$ state, most likely mediated by thermal population of the $^5D_1$ level. For **Eu·L1** and **Eu·L3** *q*, the number of coordinating solvent molecules, can be calculated and the average number of coordinating water molecules is 1 for both complexes. This indicates that the chromophore pendant arm is coordinating the lanthanide center.[25b] For **Eu·L2**, where back energy transfer is active, *q* cannot be calculated as quenching form O-H oscillators alone are not responsible for the differences in observed lifetime.[7]

Eu·L1 and Eu·L2 as luminescent probes

The key photophysical properties of the complexes are compiled in Table 5. The quantum yield for the organic fluorescence (ϕ_{fl}) and the Eu(III)-centered emission excited through the antenna (Φ_{lum}) were determined by using coumarin-153 as a known reference, following the established procedure that use five different concentrations for both sample and reference as recommended by IUPAC.[38] The Eu(III) luminescence quantum yields were found to be in the range of 0.5-3 %. For luminescent probes it is important to contrast the quantum yield to the molar absorption coefficient in order to evaluate the efficiency of the complex as a probe. This can be evaluated as the brightness ($B = \varepsilon(\lambda_{ex}) \cdot QY$). While the brightness of **Eu·L1** and **Eu·L2** are low compared to organic fluorophores (~100 vs ~100.000), it is greatly improved when compared to a Eu(III) complex with no antenna appended. Compared to EuDOTA an increase of a factor 10.000-100.000 is observed.[39] Note that **Eu·L2** has the lowest brightness of the complexes at the primary absorption maximum, but the highest brightness at 405 nm. Due to the redshift in absorption, **Eu·L2** becomes the brightest luminescent probe.

Table 6: Relative change in ligand fluorescence and Eu(III) luminescence after addition of 20 mg/mL BSA.

	I(with BSA)/I(in buffer)	
	Em_{Ligand}	Em_{Eu}
Eu·L1	0.26	0.43
Eu·L2	0.89	3.56
Eu·L3	1.29	0.56

In biological samples, binding of proteins will change the property of luminescent probes.[40] This was investigated by incremental addition of bovine serum albumin (BSA) to **Eu·L1**, **Eu·L2**, and **Eu·L3** while maintaining constant concentration of the complex, see supporting information. The results are summarized in Table 6. For **Eu·L1** and **Eu·L3** the Eu(III) luminescence is reduced by half, while it for **Eu·L2** is increased 3.5-fold.

Cell imaging

Eu·L1 and **Eu·L2** were investigated for use in bioimaging. **Eu·L3** was not used as the absorption maximum is in the UV-region. The complexes were investigated with high resolution Laser Scanning Confocal Microscopy (LSCM) images recorded on a modified Leica SP5 II microscope, equipped with a SIM technique called PhMoNa.[12d] Cell uptake and co-localization studies were done for **Eu·L1** and **Eu·L2** in living mouse skin fibroblasts (NIH-3T3). Both **Eu·L1** and **Eu·L2** permeated into the NIH-3T3 cells when loaded in DMEM (Dulbecco's modified Eagle's medium) with 10% FBS (fetal bovine serum) and 1% pen strep at 37° in 5% CO_2/air. Incubation times from 2-24 hours were tested together with concentrations ranging from 12.5 μM up to 50 μM. The cells remained visible healthy over the full period of examination of up to 24 h with 50 μM loading concentration. Colocalization experiments were done using Mitotracker Green and Lysotracker Green to confirm the localization of the Eu(III) complexes in the cell. Mitotracker Green confirmed that the complexes were predominantly localized in the mitochondria (Figure 9).

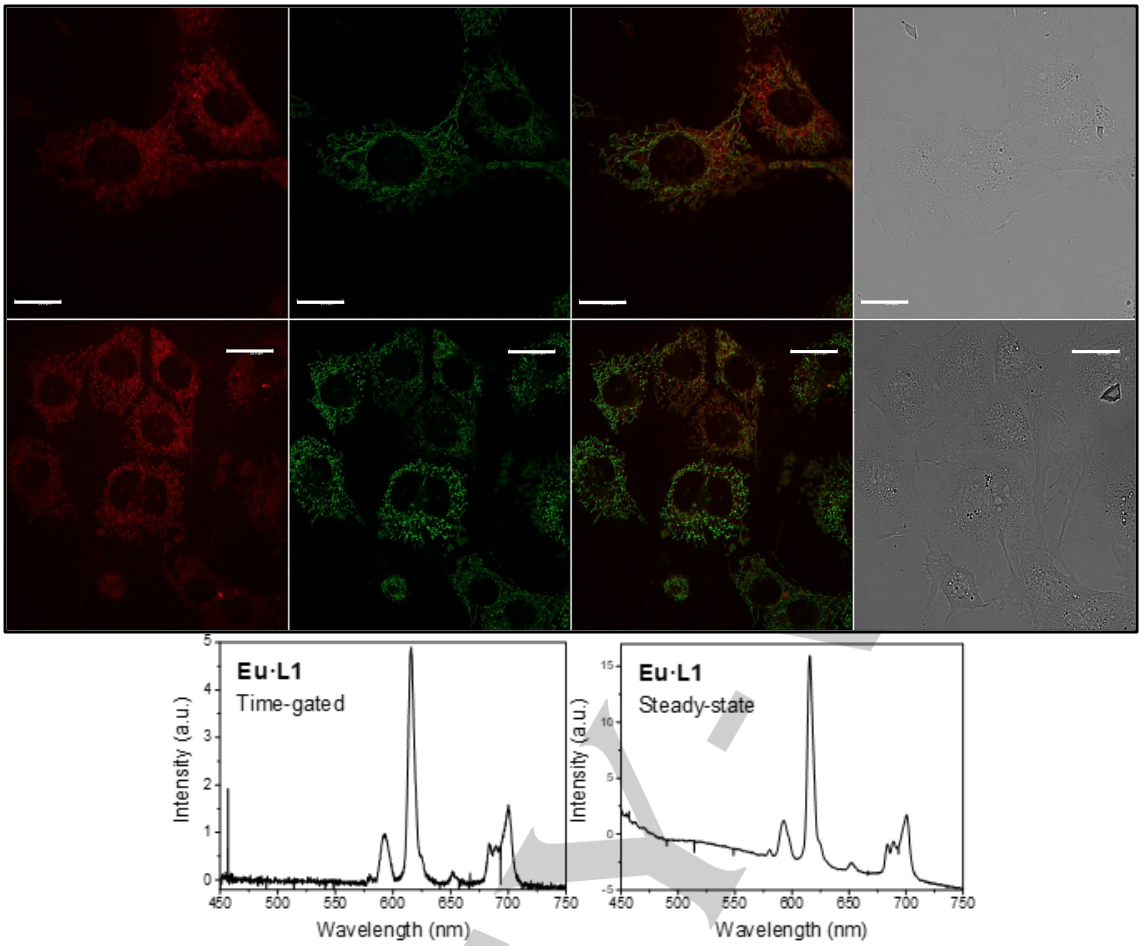

Figure 9: Top panel: 50 µM **Eu·L1** incubated for 4 h. Middle panel: 50 µM **Eu·L2** incubated for 24 h. Co-staining with mitotracker green (P = 0.74 and 0.69 respectively). Transmission images are shown for each row confirming cell viability. All cell images are obtained with 405 nm excitation. Scale bars represent to 20 µm. Bottom left: Time-gated emission spectrum of **Eu·L1** excited at 365 nm with 20 µs gate time.[12e] Bottom right: Steady-state emission spectrum of **Eu·L1** excited at 355 nm. LSCM (ref12d)

The cells stained with the two Eu(III) complexes were all excited using a 405 nm laser and the images were measured with detection from 570 -700 nm where only Eu(III) luminescence is emitted cf. Figure 9. To further confirm that the emission observed from the cells originated from the Eu(III) center, and not from the antenna or background fluorescence, time-resolved emission spectra were measured from the cells stained with **Eu·L1**: The cell slides were placed on a custom built specialized inverted microscope adapted to allow for time-gated imaging and spectroscopy.[12e] Due to instrumental limitations, these spectra were recorded using 355 nm excitation. Figure 9 shows the steady state spectrum and the time-gated spectrum, which both clearly display the Eu(III) luminescence following excitation of the ligand. These spectra confirm that **Eu·L1** permeates the cells and that the images recorded on the dedicated microscope arise from Eu(III) luminescence.

To test the luminescent probes on a conventional microscope, we used a Core Facility for Integrated Microscopy. Here, cell uptake studies were done on formaldehyde fixed HeLa cells permeabilized with Triton X-100 stained with 50 µM dye. The images were obtained using a Zeiss Confocal microscope LSM 780 where an emission profile of the luminescence detected was obtained together with the cell image using a 405 nm laser, f-MBS:405/505c or f-MBS:405/565c beam splitter, and the 32-channel detector without any additional optical elements. For **Eu·L2** no signal was obtained from the stained cells. For **Eu·L1** bright images of cell nuclei were recorded, see Figure 10A. The images obtained were compared with DAPI stained cells to confirm to localization of the complex in the nuclei, see ESI. The emission profile obtained directly from the cell images on the microscope did not reveal any Eu(III) luminescence (Figure 10B). However, when the same cover slide with the stained cells were placed in the fluorimeter, the characteristic Eu(III) luminescence with emission bands at 595 nm and 620 nm were observed (Figure 10C). This clearly demonstrates uptake of the Eu(III)-complex in the cell, and that the issue is the microscope, not the luminescent probe. These experiments were replicated with live cells with the same result.

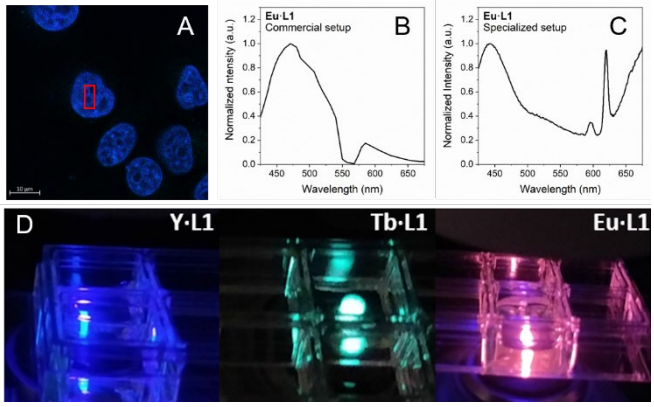

Figure 10: A: 50 μM **Eu·L1** stained cell. B: Emission profile of the luminescence collected from the nuclei (red square, A). The spectrum was obtained from LSM 780 microscope. C: Steady state emission spectrum of the same cell slide obtained from a fluorimeter. D: Image of emitted light from a 150 μM **Y·L1** **Tb·L1**, and **Eu·L1** solution in PBS. A, B, and C are using identical settings on the same microscope All images and spectra are obtained with 405 nm excitation.

The experiments done on the LSM 780 microscope indicated that the commercial setup was not able to detect the Eu(III) luminescence in cells. The laser side of the instrument was tested with solutions of **Y·L1**, **Tb·L1**, and **Eu·L1,** where the emitted light after excitation at 405 nm observed with the eye are as expected, Figure 10D. Thus, the problem seeing the Eu(III) luminescence in the microscope must be on the detector side.

ICP-MS analysis was used to confirm that the uptake of Eu(III) in the cell for both **Eu·L1** and **Eu·L2** documenting that the complexes are present in the cells. As further support—in addition to the spectra in Figure 9 and 10C—the luminescence lifetime of the **Eu·L1** complex was determined in the cells. The luminescence lifetime decreases to 99 μs in cells, significantly less than the 604 μs luminescence lifetime in PBS and also lower than the 239 μs determined in the DMEM cell media. This indicates strong quenching effects from both cell media and the cell biology, which is not unexpected since Eu(III) luminescence is strongly affected by the chemical environment,[13e, 41] but it also fully confirms the presence of complexes in the cells.

Thus, the issue must be the combination of lanthanide luminescence and microscopes tailored for use with organic fluorophores. Therefore, further optimization of the photophysics of antenna chromophore appended lanthanide complexes are required before lanthanide based probes can be directly applied in optical bioimaging.[10]

Conclusions

Three sets of four lanthanide(III) complexes were synthesized, characterized and their photophysics was investigated in great detail. The Eu(III) complexes were investigated as lanthanide based luminescent probes. While high quality images of the mitochondria was recorded using Eu(III) luminescence on a dedicated microscope, no Eu(III) luminescence was recorded on conventional commercial microscopes. It was clearly shown that europium(III) was present in the investigated cell samples, and did luminesce in the cells. Thus, we conclude that at the current state of development, conventional fluorescence microscopes are not suitable platforms for lanthanide based bioimaging and further development of the lanthanide complexes must be done. The results from our detailed investigation of these complexes showed that the devil is in the intricate details of structure, kinetics, and energetics. Details that are so intricate that our conclusion is that the theory predicting the performance of a lanthanide based probe in a biological samples are yet to be developed.

Conflicts of interest

There are no conflicts to declare.

Acknowledgements

We acknowledge the Core Facility for Integrated Microscopy, Faculty of Health and Medical Sciences, University of Copenhagen. We thank the Carlsberg foundation, Villum Fonden, Novo Nordisk Fonden, Eliteforsk, and the University of Copenhagen for generous support. We thank Stefan Warthegau for assistance in the preparation of the manuscript.

Keywords: Lanthanide complexes • Luminescence • Photophysics • Bioimaging • f-elements

[1] P. Montero Llopis, R. A. Senft, T. J. Ross-Elliott, R. Stephansky, D. P. Keeley, P. Koshar, G. Marqués, Y.-S. Gao, B. R. Carlson, T. Pengo, M. A. Sanders, L. A. Cameron, M. S. Itano, *Nature Methods* **2021**, *18*, 1463-1476.

[2] a) D. L. Farkas, *Nat Biotech* **2003**, *21*, 1269-1271; b) D. J. Stephens, V. J. Allan, *Science* **2003**, *300*, 82-86; c) S. W. Hell, *Science* **2007**, *316*, 1153-1158; d) N. Johnsson, K. Johnsson, *ACS Chem. Bio.* **2007**, *2*, 31-38.

[3] a) L. D. Lavis, R. T. Raines, *ACS Chem. Biol.* **2008**, *3*, 142-155; b) R. P. Haugland, *Handbook of Fluorescent Probes and Research Chemicals*, 11th ed., Molecular Probes, Eugene, Oregon, **2010**; c) J. B. Grimm, L. D. Lavis, *Nature Methods* **2022**, *19*, 149-158; d) E. A. Specht, E. Braselmann, A. E. Palmer, *Annual Review of Physiology* **2017**, *79*, 93-117; e) B. N. G. Giepmans, S. R. Adams, M. H. Ellisman, R. Y. Tsien, *Science* **2006**, *312*, 217-224.

[4] K. H. Drexhage, *Top. Appl. Phys.* **1973**, *1*, 144-193.

[5] a) W.-C. Sun, K. R. Gee, D. H. Klaubert, R. P. Haugland, *The Journal of Organic Chemistry* **1997**, *62*, 6469-6475; b) N. Panchuk-Voloshina, R. P. Haugland, J. Bishop-Stewart, M. K. Bhalgat, P. J. Millard, F. Mao, W. Y. Leung, *J. Histochem. Cytochem.* **1999**, *47*, 1179-1188.

[6] J. B. Grimm, A. K. Muthusamy, Y. Liang, T. A. Brown, W. C. Lemon, R. Patel, R. Lu, J. J. Macklin, P. J. Keller, N. Ji, L. D. Lavis, *Nat Methods* **2017**, *14*, 987-994.

[7] a) G. Vereb, E. Jares-Erijman, P. R. Selvin, T. M. Jovin, *Biophys J* **1998**, *74*, 2210-2222; b) S. Faulkner, A. Beeby, R. S. Dickins, D. Parker, J. A. G. Williams, *Journal of fluorescence* **1999**, *9*, 45-49; c) A. Beeby, S. W. Botchway, I. M. Clarkson, S. Faulkner, A. W. Parker, D. Parker, J. A. G. Williams, *Journal of Photochemistry and Photobiology B-Biology* **2000**, *57*, 83-89; d) S. I. Weissman, *The Journal of chemical physics* **1942**, *10*, 214-217; e) H. B. Beverloo, A. van Schadewijk, S. van Gelderen-Boele, H. J. Tanke, *Cytometry* **1990**, *11*, 784-792; f) A. D. Elster, S. C. Jackels, N. S. Allen, R. C. Marrache, *American Journal of Neuroradiology* **1989**, *10*, 1137. g) M. Tropiano, O. A. Blackburn, J. A. Tilney, L. R. Hill, T. Just Sørensen, S. Faulkner, *Journal of Luminescence* **2015**, *167*, 296-304.

[8] a) P. R. Selvin, *Annu Rev Biophys Biomol Struct* **2002**, *31*, 275-302; bM. C. Heffern, L. M. Matosziuk, T. J. Meade, *Chem Rev* **2014**, *114*, 4496-4539; c) J. C. Bunzli, *Chem Rev* **2010**, *110*, 2729-2755; d) C. P. Montgomery, B. S. Murray, E. J. New, R. Pal, D. Parker, *Acc Chem Res* **2009**, *42*, 925-937; e) E. G. Moore, A. P. Samuel, K. N. Raymond, *Acc Chem Res* **2009**, *42*, 542-552; f) L. D. Sun, Y. F. Wang, C. H. Yan, *Acc Chem Res* **2014**, *47*, 1001-1009; gL. Francés-Soriano, N. Hildebrandt, L. J. Charbonnière, in *Reference Module in Chemistry, Molecular Sciences and Chemical Engineering*, Elsevier, **2022**.

[9] S. J. Butler, L. Lamarque, R. Pal, D. Parker, *Chemical Science* **2014**, *5*, 1750-1756.

[10] T. J. Sørensen, S. Faulkner, in *5 Lanthanide Complexes Used for Optical Imaging* (Eds.: S. Astrid, F. Eva, K. O. S. Roland), De Gruyter, **2021**, pp. 137-156.

[11] M. Kleinerman, *The Journal of chemical physics* **1969**, *51*, 2370-2381.

[12] a) A. Nonat, S. Bahamyirou, A. Lecointre, F. Przybilla, Y. Mely, C. Platas-Iglesias, F. Camerel, O. Jeannin, L. J. Charbonniere, *Journal of the American Chemical Society* **2019**, *141*, 1568-1576; b) Z. Liao, M. Tropiano, S. Faulkner, T. Vosch, T. J. Sørensen, *RSC Adv.* **2015**,

70282–70286; c) Z. Liao, M. Tropiano, K. Mantulnikovs, S. Faulkner, T. Vosch, T. Just Sørensen, *Chemical Communications* **2015**, *51*, 2372-2375; d) R. Pal, *Faraday Discussions* **2015**, *177*, 507-515; e) R. Pal, A. Beeby, *Methods and applications in fluorescence* **2014**, *2*, 037001; f) P. Stachelek, L. MacKenzie, D. Parker, R. Pal, *Nature Communications* **2022**, *13*, 553.

[13] a) A. Picot, A. D'Aléo, P. L. Baldeck, A. Grichine, A. Duperray, C. Andraud, O. Maury, *Journal of the American Chemical Society* **2008**, *130*, 1532-1533; b) J. H. Yu, D. Parker, R. Pal, R. A. Poole, M. J. Cann, *Journal of the American Chemical Society* **2006**, *128*, 2294-2299; c) S. Petoud, S. M. Cohen, J. C. G. Bunzli, K. N. Raymond, *Journal of the American Chemical Society* **2003**, *125*, 13324-13325; d) A. Foucault-Collet, K. A. Gogick, K. A. White, S. Villette, A. Pallier, G. Collet, C. Kieda, T. Li, S. J. Geib, N. L. Rosi, S. Petoud, *Proceedings of the National Academy of Sciences of the United States of America* **2013**, *110*, 17199-17204; e) D. Kovacs, X. Lu, L. S. Meszaros, M. Ott, J. Andres, K. E. Borbas, *Journal of the American Chemical Society* **2017**, *139*, 5756-5767; f) E. Pershagen, K. E. Borbas, *Angewandte Chemie* **2015**, *54*, 1787-1790; g) K. E. Martin, A. G. Cosby, E. Boros, *Journal of the American Chemical Society* **2021**, *143*, 9206-9214; h) M. Cardoso Dos Santos, I. Colin, G. Ribeiro Dos Santos, K. Susumu, M. Demarque, I. L. Medintz, N. Hildebrandt, *Advanced Materials* **2020**, *32*, 2003912.

[14] R. Xiong, D. Mara, J. Liu, R. Van Deun, K. E. Borbas, *Journal of the American Chemical Society* **2018**, *140*, 10975-10979.

[15] J. Icha, M. Weber, J. C. Waters, C. Norden, *Bioessays* **2017**, *39*.

[16] M. R. Carro-Temboury, R. Arppe, C. Hempel, T. Vosch, T. Just Sørensen, *Plos One* **2017**, *12*, e0189529.

[17] R. Arppe-Tabbara, M. R. Carro-Temboury, C. Hempel, T. Vosch, T. J. Sørensen, *Chemistry – A European Journal* **2018**, *24*, 11885-11889.

[18] a) T. J. Sørensen, S. Faulkner, *Acc Chem Res* **2018**, *51*, 2493-2501; b) P. Caravan, J. J. Ellison, T. J. McMurry, R. B. Lauffer, *Chemical Reviews* **1999**, *99*, 2293-2352; c) J. Wahsner, E. M. Gale, A. Rodríguez-Rodríguez, P. Caravan, *Chemical Reviews* **2019**, *119*, 957-1057.

[19] a) M. J. S. Dewar, *Journal of the Chemical Society* **1950**, 2329-2334; bJ. Griffiths, *Colour and Constitution of Organic Molecules*, Academic Press, **1976**; cA. K. R. Junker, T. J. Sørensen, *Methods and Applications in Fluorescence* **2017**, *6*, 014002.

[20] a) P. Atkinson, K. S. Findlay, F. Kielar, R. Pal, D. Parker, R. A. Poole, H. Puschmann, S. L. Richardson, P. A. Stenson, A. L. Thompson, J. Yu, *Organic & Biomolecular Chemistry* **2006**, *4*, 1707-1722; b) P. Verma, R. M. Sawant, H. Pal, *Physical Chemistry Chemical Physics* **2015**, *17*, 23214-23225.

[21] D. Parker, R. Pal, J. Yu, *Vol. United States Patent No: US 8,193,174 B2* . Google Patents, **2012**.

[22] a) T. J. Sørensen, M. Tropiano, O. A. Blackburn, J. A. Tilney, A. M. Kenwright, S. Faulkner, *Chem Commun (Camb)* **2013**, *49*, 783-785; b) T. J. Sørensen, A. M. Kenwright, S. Faulkner, *Chemical Science* **2015**, *6*, 2054-2059.

[23] a) L. G. Nielsen, T. J. Sørensen, *Inorganic Chemistry* **2019**, *59*, 1, 94-105; b) V. Jacques, J. F. Desreux, *Inorganic Chemistry* **1994**, *33*, 4048-4053; c) J. F. Desreux, *Inorganic Chemistry* **1980**, *19*, 1319-1324; d) S. Aime, M. Botta, G. Ermondi, *Inorganic Chemistry* **1992**, *31*, 4291-4299; e) S. Aime, M. Botta, M. Fasano, M. P. M. Marques, C. F. G. C. Geraldes, D. Pubanz, A. E. Merbach, *Inorganic Chemistry* **1997**, *36*, 2059-2068.

[24] A. K. Junker, M. Tropiano, S. Faulkner, T. J. Sorensen, *Inorganic Chemistry* **2016**, *55*, 12299-12308.

[25] a) A. K. R. Junker, L. R. Hill, A. L. Thompson, S. Faulkner, T. J. Sørensen, *Dalton transactions* **2018**, *47*, 4794-4803; b) A. K. R. Junker, T. J. Sørensen, *Dalton Transactions* **2019**, *48*, 964-970.

[26] R. Arppe, N. Kofod, A. K. R. Junker, L. G. Nielsen, E. Dallerba, T. Just Sørensen, *European Journal of Inorganic Chemistry* **2017**, 5246-5253.

[27] L. G. Nielsen, A. K. R. Junker, T. J. Sørensen, *Dalton transactions* **2018**, *47*, 10360-10376.

[28] J. R. Lakowicz, *Principles of fluorescence spectroscopy*, 3. ed. ed., Springer, New York, **2006**.

[29] a) W. Carnall, P. Fields, K. Rajnak, *The Journal of Chemical Physics* **1968**, *49*, 4450-4455; b) W. Carnall, P. Fields, K. Rajnak, *The Journal of Chemical Physics* **1968**, *49*, 4447-4449; cW. Carnall, P. Fields, K. Rajnak, *The Journal of Chemical Physics* **1968**, *49*, 4443-4446.

[30] T. Aruga, O. Ito, M. Matsuda, *Journal of the American Chemical Society* **1979**, *101*, 7585-7589.

[31] aC. Würth, M. Grabolle, J. Pauli, M. Spieles, U. Resch-Genger, *Nature Protocols* **2013**, *8*, 1535-1550; bA. M. Brouwer, **2011**, *83*, 2213-2228.

[32] N. Kofod, P. Nawrocki, T. J. Sørensen, *The Journal of Physical Chemistry Letters* **2022**, *13*, 3096-3104.

[33] N. Kofod, T. J. Sørensen, *The Journal of Physical Chemistry Letters* **2022**, *13*, 11968-11973.

[34] L. G. Nielsen, T. J. Sørensen, *Methods and Applications in Fluorescence* **2023**, *11*, 015005.

[35] R. Arppe, N. Kofod, A. K. R. Junker, L. G. Nielsen, E. Dallerba, T. Just Sørensen, *European Journal of Inorganic Chemistry* **2017**, *2017*, 5246-5253.

[36] K. Binnemans, *Coordination Chemistry Reviews* **2015**, *295*, 1-45.

[37] a) R. M. Supkowski, W. D. Horrocks Jr, *Inorganica Chimica Acta* **2002**, *340*, 44-48; b) A. Beeby, I. M. Clarkson, R. S. Dickins, S. Faulkner, D. Parker, L. Royle, A. S. de Sousa, J. A. Gareth Williams, M. Woods, *Journal of the Chemical Society, Perkin Transactions 2* **1999**, 493-504.

[38] a) C. Würth, M. Grabolle, J. Pauli, M. Spieles, U. Resch-Genger, *Nat. Protocols* **2013**, *8*, 1535-1550; b) A. M. Brouwer, *Pure Appl. Chem.* **2011**, *83*, 2213-2228; c) U. Resch-Genger, K. Hoffmann, W. Nietfeld, A. Engel, J. Neukammer, R. Nitschke, B. Ebert, R. Macdonald, *Journal of Fluorescence* **2005**, *15*, 337-362.

[39] manuscript in preperation

[40] a) G.-L. Law, C. Man, D. Parker, J. W. Walton, *Chemical Communications* **2010**, *46*, 2391-2393; b) X. Wang, X. Wang, Y. Wang, Z. Guo, *Chemical Communications* **2011**, *47*, 8127-8129; c) R. Mailhot, T. Traviss-Pollard, R. Pal, S. J. Butler, *Chemistry – A European Journal* **2018**, *24*, 10745-10755.

[41] a) D. Kovacs, K. E. Borbas, *Coordination Chemistry Reviews* **2018**, *364*, 1-9; b) D. Kovacs, E. Mathieu, S. R. Kiraev, J. A. L. Wells, E. Demeyere, A. Sipos, K. E. Borbas, *Journal of the American Chemical Society* **2020**, *142*, 13190-13200.

Entry for the Table of Contents

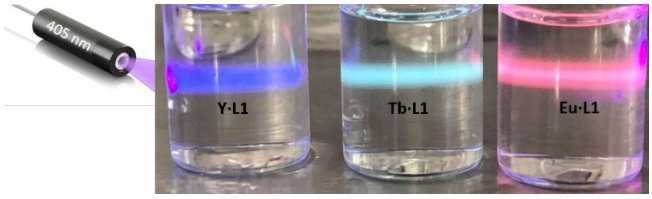

Lanthanide luminescence can attain significant brightness in antenna chromophore appended complexes, but how bright can it be? And is it enough for conventional bioimaging? In this study we explore both photophysics and bioimaging of three antenna appended lanthanide complexes

Institute and/or researcher Twitter usernames: @f_elements @lanthanides_cph @CHEMUCPH